Ultrasonic characterization of the nonlinear properties of canine livers by measuring shear wave speed and axial strain with increasing portal venous pressure

Veronica Rotemberg [a,*], Brett Byram [a], Mark Palmeri [a,b], Michael Wang [a],
Kathryn Nightingale [a]

[a] Department of Biomedical Engineering, Duke University, Room 136 Hudson Hall, Box 90281, Durham, NC 27708, USA
[b] Department of Anesthesiology, Duke University Medical Center, Durham, NC, USA

A B S T R A C T

Elevated hepatic venous pressure is the primary source of complications in advancing liver disease. Ultrasound imaging is ideal for potential noninvasive hepatic pressure measurements as it is widely used for liver imaging. Specifically, ultrasound based stiffness measures may be useful for clinically monitoring pressure, but the mechanism by which liver stiffness increases with hepatic pressure has not been well characterized. This study is designed to elucidate the nonlinear properties of the liver during pressurization by measuring both hepatic shear wave speed (SWS) and strain with increasing pressure. Tissue deformation during hepatic pressurization was tracked in 8 canine livers using successively acquired 3-D B-mode volumes and compared with concurrently measured SWS. When portal venous pressure was increased from clinically normal (0–5 mmHg) to pressures representing highly diseased states at 20 mmHg, the liver was observed to expand with axial strain measures up to 10%. At the same time, SWS estimates were observed to increase from 1.5–2 m/s at 0–5 mmHg (baseline) to 3.25–3.5 m/s at 20 mmHg.

© 2013 Elsevier Ltd. All rights reserved.

1. Introduction

Increasing portal venous pressure (PVP) is one of the hallmarks of advancing liver disease and contributes to leading causes of death and morbidity from cirrhosis, such as variceal hemorrhage (Ripoll et al., 2007; Gulzar et al., 2009; Sharara and Rockey, 2001). Increasing pressure in the portal vein, which is the primary source of blood flow to the liver, is typically referred to as elevated hepatic or PVP. Monitoring hemodynamic response to therapies for reducing hepatic pressure through use of hepatic venous pressure gradient (HVPG) measurement has proven effective in prolonging life, but is expensive and invasive (Imperiale, 2003). Ultrasound imaging has been widely used for imaging the liver and gallbladder (Wu, 2008) and therefore is ideal for potential noninvasive hepatic pressure measurements. Duplex Doppler ultrasonography has been previously proposed for HVPG estimation (Yang, 2007; Zironi et al., 1992; Wu, 2008) and has shown a clear relationship between quantitative results and esophageal varices development (Bolondi and Gaiani, 1994). However, this method is not sufficiently accurate or reproducible between observers for implementation in clinical practice for HVPG quantification (Bolondi et al., 1991; Vries et al., 1991; Vizzutti et al., 2008). Ultrasound and MRI-based estimates of liver stiffness have been reported to increase with hepatic pressure (Millonig et al., 2010; Vizzutti et al., 2008; Bureau et al., 2008; Robic et al., 2011; Yin et al., 2011), suggesting that stiffness-based approaches may provide the basis for a noninvasive and inexpensive approach toward characterizing portal vein pressure in the clinic. These include splenic stiffness measurements (Takuma et al., in press; Nedredal et al., 2011) and direct liver stiffness measures (Robic et al., 2011; Han et al., 2012).

The major challenge to noninvasive stiffness-based metrics for characterizing hepatic pressure in vivo is that estimates of hepatic stiffness are also known to increase from a SWS of 1–1.5 m/s for normal livers to 3.5–5 m/s to with advanced fibrosis stage (Takuma et al., in press; Robic et al., 2011; Palmeri et al., 2011; Friedrich-Rust et al., 2008; Yoneda et al., 2008; Bavu et al., 2011; Crespo et al., 2012; Schlosser et al., 2009). While splenic stiffness has also been observed to increase with esophageal varices risk and PVP, splenic stiffness is also increased from baseline in patients with cirrhosis and without high levels of esophageal varices risk (Takuma et al., in press). Thus, a better understanding of the mechanisms by which hepatic pressure modulates estimates of liver stiffness could provide information needed to distinguish

* Corresponding author. Tel.: +1 919 660 5223.
E-mail address: veronica.rotemberg@duke.edu (V. Rotemberg).

increasing hepatic pressure from advancing fibrosis stage. We have previously reported the nonlinear hyperelastic behavior of the liver as PVP increases (Rotemberg et al., 2012). In this work, an experiment was designed to simultaneously measure changes in hepatic strain and stiffness with increasing hepatic pressure in excised canine livers.

2. Background

This work primarily focuses on the potential applications of nonlinear characterization of the liver using shear wave speed (SWS) metrics toward noninvasive hepatic pressure characterization. Nonlinear properties of the liver have previously been explored for the purpose of computational surgery guidance (Jordan et al., 2009) and modeling car accident injury (Brunon et al., 2010) as well as development of power law based models for soft tissues (Nicolle et al., 2010). Nonlinear mechanical property evaluation of soft tissues such as the liver often requires information about corresponding stress and strain at particular time points. In the pressurized liver, because the geometry is so complicated, it is not feasible to translate the PVP directly into a stress without many simplifying assumptions. However, it is of clinical interest for potential applications of noninvasive pressure characterization to characterize the nonlinear mechanical properties that determine the increase in liver stiffness corresponding to PVP increases. The experiments described herein are inspired by acoustoelasticity experiments in that they generate estimates of SWS and applied strain (Gennisson et al., 2007; Shams et al., 2011), but novel in that both the applied strain and the resulting SWS increase are measured using ultrasonic metrics in response to an unknown applied stress in the form of PVP.

3. Methods

3.1. Experimental animals

Experimental excised canine livers were obtained through cooperation with the Duke University Vivarium and euthanasia was achieved within the guidelines provided by the Duke Institutional Animal Care and Use Committee. Imaging was performed within 2 h of excision and 3 mL of heparin were administered prior to euthanasia in 7 of the 8 cases to reduce coagulation effects.

### 3.2. Evaluation of hepatic changes with pressurization

The experiments described were designed to compare changes in hepatic deformation and stiffness estimates with increasing PVP. Eight excised canine livers were investigated. After the canine liver was removed, the hepatic artery, hepatic vein, and portal vein were cannulated and the hepatic artery and vein were closed.

In all livers, super glue (Loctite® Westlake, OH) was used to seal any observed defects in the liver capsule due to the liver extraction (all defects were < 2 mm). The liver was then placed in a heparinized saline bath for 5 min to remove remaining air in the liver. We attempted to mitigate the effects of included air, saline leakage, and clotting, because all could contribute to decreased observed strain and stiffness response to increasing hepatic pressure.

Increasing PVP was achieved by attachment of the portal vein to a variable height saline reservoir as described in (Rotemberg et al., 2012). A diagram of the experimental setup is shown in Fig. 1.

In order to characterize hepatic expansion, the livers were allowed to expand in a heparinized saline bath throughout the experiment. Liver pressure was increased stepwise from 0 to 20 mmHg with pressurization steps at 0.5–5 mmHg in magnitude as measured using a handheld digital manometer (SPER Scientific, Ltd., resolution=0.075 mmHg) attached to the portal vein cannulation setup. During each pressurization step, 3-D B-mode datasets were acquired using a Siemens Acuson SC2000™ scanner and 4Z1c matrix array ((Frey and Chiao, 2008) Siemens Healthcare, Mountain View, CA, USA). The 3-D B-mode volumes were acquired with a frame rate of 0.1 Hz for up to 4 min over a $2 \times 1.2 \times 1.2$ cm^3 volume located 5–7 cm axially away from the transducer.

Fig. 2 shows a single A-line through time from the 4-D dataset acquired for one pressurization increment. After each pressurization step, 6 SWS datasets were acquired with a separate system as described below from the region corresponding to that in which the 3-D B-mode acquisition occurred.
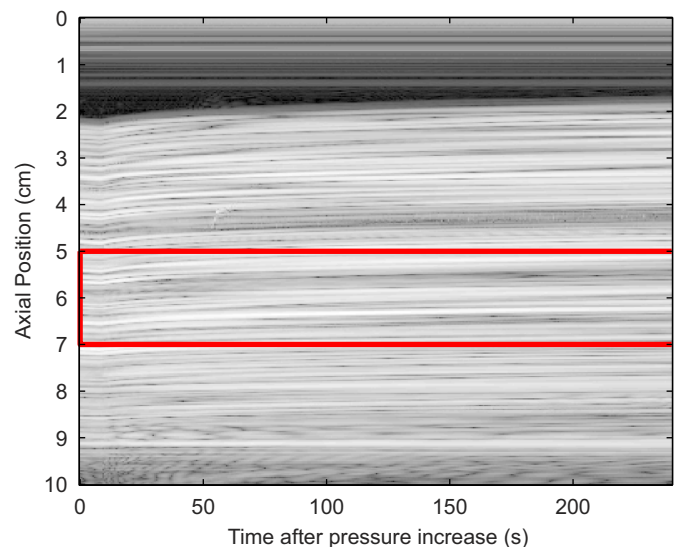
Fig. 2. Example of data acquired in a pressurization increment between 17 and 18 mmHg PVP in one excised canine liver. One axial A-line through the center of the volume interrogated is shown through time after pressure increase. Expansion is observed in the growth of the brighter region, which represents the liver. The red lines represent the axial extent of the 3-D region of interest over which strain was computed. (For interpretation of the references to color in this figure legend, the reader is referred to the web version of this article.)
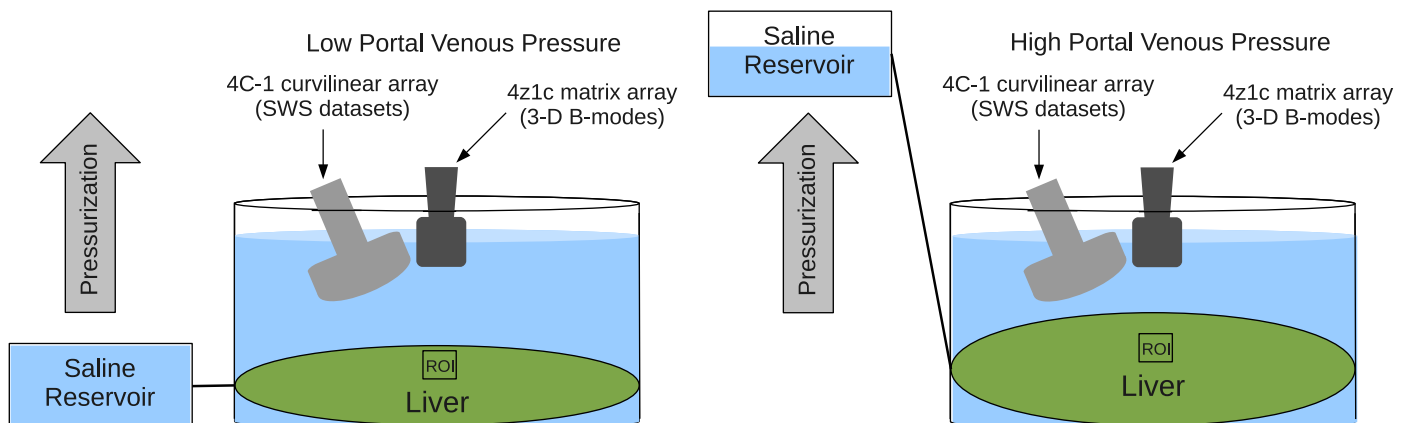
Fig. 1. Diagram of the hepatic pressurization and monitoring setup.

3.3. Three-dimensional displacement estimation

Because the liver expansion occurs in all directions, a 3-D displacement estimation kernel and search region were used to determine the axial displacements used for calculation of axial strain. Axial displacements were estimated using phase-sensitive 3-D cross correlation (Embree and O'Brien, 1985; Wear and Popp, 1987). Phase-sensitive normalized cross correlation with grid slopes algorithm sub-sample estimation was implemented as described in by Byram et al. (2010). A 0.9 correlation coefficient cutoff was implemented for the displacement estimates. Details of the displacement estimation parameters for hepatic deformation quantification can be found in Table 1.

These parameters are consistent with the kernel sizes and dimensions previously reported for strain imaging in 2-D (Konofagou et al., 2011; Korukonda and Doyley, 2011; Wang et al., 2008) and 3-D displacement estimation (Byram et al., 2010; Kuo and von Ramm, 2008).
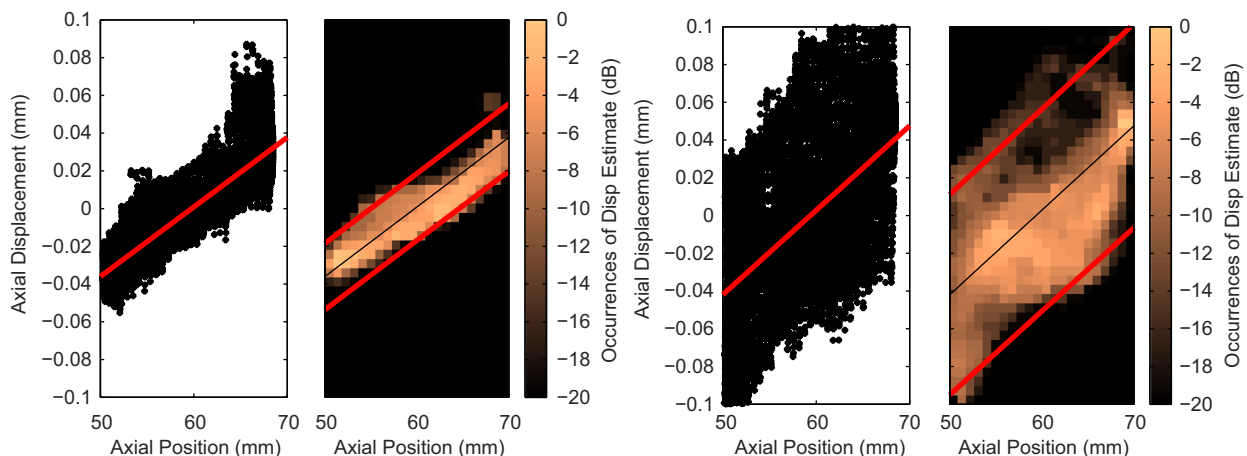
3.4. Strain calculation

In order to characterize the change in hepatic strain through time, the Eulerian description (Hjelmstad, 2005) was utilized in that a fixed region of interest was interrogated using ultrasound based techniques and the tissue strains calculated through time in that region were accumulated to generate a quantitative estimate of the change in hepatic deformation between different pressurization states. The Eulerian Strain Tensor (e_{ij}) is defined in the following equation using the spatial derivative of the displacement (Hjelmstad, 2005).

$$e_{ij} = \frac{1}{2}\left(\frac{\partial u_i}{\partial x_j} + \frac{\partial u_j}{\partial x_i} - \frac{\partial u_m}{\partial x_i}\frac{\partial u_m}{\partial x_j}\right) \tag{1}$$

In Eq. (1), u_i represent the 3-D displacements calculated between B-mode volumes, and x_i are spatial coordinates at which the displacements are measured.

Table 1
Parameters used for 3-D displacement estimation.

Parameter	Value
Ultrasound scanner	Siemens Acuson SC2000™
Probe	4Z1c
F_c (MHz)	2.8
Transmit focus (cm)	8
Imaging depth (cm)	5–7
Volume rate (Hz)	0.1
Axial kernel (mm)	2.88
Lateral kernel (mm)	0.60
Elevational kernel (mm)	0.68

The low center frequency of the matrix transducer used (2.8 MHz) and small aperture did not allow for estimation of lateral or elevational strains for this experimental system (Righetti et al., 2003). The axial strain (e_{11}) was calculated using a least-squares fit to the axial displacement estimates in the region of interest as a function of axial position (Kallel et al., 1996; Kallel and Ophir, 1997). This is an approximation to the derivative of the axial strain as a function of axial position, where the strain in the region of interest is assumed to be constant. Strains calculated were limited to below 0.45% strain in each calculation of e_{11}, so the infinitesimal strain assumption holds for each calculation (Hjelmstad, 2005) and cross terms were excluded. In Eq. (1), the calculation of strain considers a zero strain initial state but the incremental strains calculated in this experiment were changes in strain from each sequential reference volume. Thus, Eqs. (2) and (3) show the calculations that were used for each incremental strain calculation ($\Delta_{e_{11}}$) and for the accumulated axial strain estimate (e_p). Eq. (3) represents a discrete integral of the strains calculated up to a particular pressure state, A.

$$\Delta_{e_{11}} = \left(\frac{\partial u_1}{\partial x_1}\right) \tag{2}$$

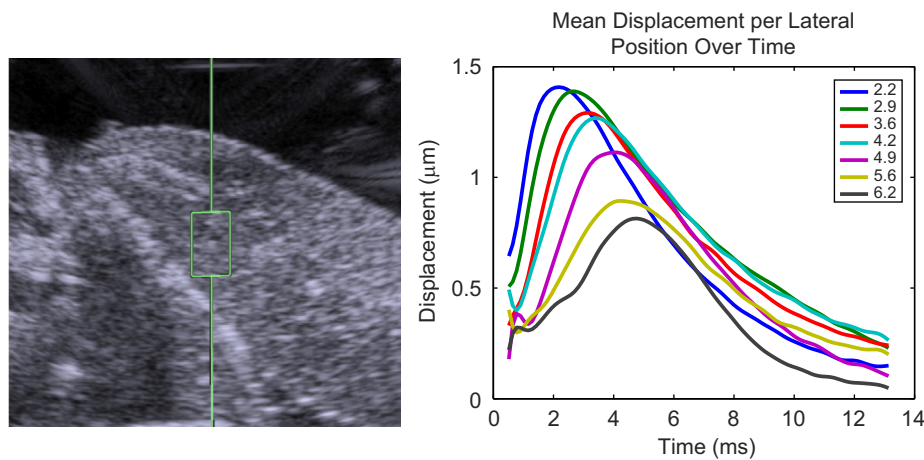$$e_{p=A} = \int_0^A \frac{\Delta_{e_{11}}}{\Delta_p}\,dp \tag{3}$$

Two examples of the incremental strain calculation ($\Delta_{e_{11}}$) between two volumes over the entire region of interest are shown in Fig. 3. For each pressurization increment, displacement estimates were acquired for 2–4 min at a rate between 0.1 Hz and 1.5 Hz. The volume rate was maintained so that all strains calculated were less than 0.45% as simulations of this experimental setup showed significant peak hopping for strain states above this value.

3.5. SWS estimation methods

Tissue stiffness was quantified using standard shear wave imaging methods (Sarvazyan et al., 1998; Nightingale et al., 2003). Radiation force-induced displacements were estimated from in-phase and quadrature (IQ) data offline using Loupas' phase-shift estimator (Pinton et al., 2006; Loupas et al., 1995). The time of the peak displacement at each lateral position was used to identify the arrival time for SWS approximation (Palmeri et al., 2008; Sandrin et al., 2002) as shown in Fig. 4. Shear waves were generated via acoustic radiation force using a Siemens Acuson SC2000™ scanner and 4C-1 curvilinear array using the Siemens quantitative elasticity imaging tool with post-processing of the IQ data performed offline (Rotemberg et al., 2012). Displacements between 1.4 and 8 mm lateral to the radiation force excitation were used to generate SWS estimates using a RANSAC-based time-of-flight algorithm (Wang et al., 2010). The SWS measures were calculated at each pressurization increment but were not accumulated.

Under the commonly used assumptions of linear elasticity and incompressibility, the relationship between SWS, the tissue shear modulus (μ), and the material density (ρ) are related by the following equation (Lai et al., 1999).

$$SWS = \sqrt{\frac{\mu}{\rho}} \tag{4}$$

Fig. 3. Axial strain calculation was performed using linear regression between axial displacement and axial position throughout the imaging volume for each time step (14,080 kernels/volume). Subplots (a) and (b) provide example results from similar strain states in two different livers but with very different 95% confidence intervals on the strain estimate. In the left of each subfigure, all the displacement estimates used to perform the linear regression are shown while on the right the distribution of displacement estimates at each axial position is shown. The red lines on the right side of each subfigure show the bounds of the 95% confidence interval of the linear regression. In subfigure (a), the strain was 0.37% with the confidence interval of 0.03% while in subfigure (b), the strain was 0.45% and the confidence interval was 0.1%. In order to maintain strain magnitudes below 0.45% strain between two volumes, the repetition rate for B-mode volume acquisitions was increased. (For interpretation of the references to color in this figure legend, the reader is referred to the web version of this article.)

Fig. 4. Sample SWS dataset acquisition region (left) and radiation force induced displacements (right). Each colored line represents a different lateral position, and the SWS can be calculated by observing the arrival time shift as the wave propagates laterally. Displacements were averaged over 0.8 mm axially (the extent of the green box on the left) in a sample hepatic dataset and a 1000 Hz low-pass filter has been applied to displacements in the temporal dimension in the right image to reduce the effects of small amplitude variation of the displacement. (For interpretation of the references to color in this figure legend, the reader is referred to the web version of this article.)

However, these assumptions do not predict changes in SWS with increasing pressure or hepatic strain so they are not sufficient for describing the strain-dependent increase in SWS measures with hepatic pressure that has been previously observed (Rotemberg et al., 2012).

$$SWS = f(e_p, \mu_1 \ldots, \mu_N) \tag{5}$$

The experiments herein are devoted to further clarifying the relationship between SWS and strain by comparing the SWS and strain measures with increasing hepatic PVP (as described by Eq. (5) in which the μ_N represent an unknown quantity of material parameters that may be required).

4. Results

The comparison between SWS and strain estimates in pressurized livers was performed in order to evaluate the relationship between strain and stiffness in a material with known nonlinear mechanical properties and irregular geometry. Ultrasound based estimates of tissue stiffness and axial strain were acquired in the same region to develop a better understanding of tissue nonlinear properties. These nonlinear properties dictate the response of the liver to increasing PVP and may provide the basis for a noninvasive method for pressure measurement in the future.

Fig. 5 shows an example of the strain accumulation process for one pressurization increment. An increase of 3.5% axial strain was observed during an increase in PVP from 10.2 to 12.5 mmHg. The red markers show the summed axial strain while the error bars on the red line in the figure represent the summed 95% confidence intervals on each strain fit shown in blue.

Increases in SWS estimates and axial strain were observed with increasing PVP in six of the eight canine livers interrogated (Fig. 6, bottom left). SWS error bars represent the standard deviation of 6 repeated measures in the same region of interest in a given liver while no percent axial strain error bars are shown to represent that each is a single measure of accumulated strain.

In two livers, there were no increases in percent axial strain with pressurization (Fig. 6, top row). In each of the canine livers examined, increases in SWS measures were associated with corresponding increases in estimates of percent axial strain. This relationship for the 6 cases in which both were observed to increase is shown in Fig. 6.

5. Discussion

Increasing hepatic venous pressure is associated with advanced liver disease and worsening patient outcomes (Sharara and
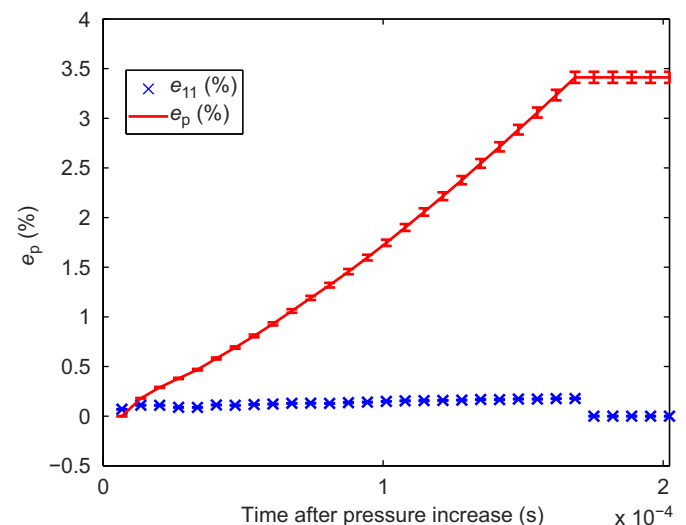

Fig. 5. Accumulated axial strain (red) during a pressurization increment between 10.4 and 12.5 mmHg as estimated using accumulation of individual volume-to-volume strain calculations (blue). The error bars shown are the accumulated 95% confidence intervals on the strain estimates. (For interpretation of the references to color in this figure legend, the reader is referred to the web version of this article.)

Rockey, 2001). It has been shown that pharmacologically lowering and tracking portal pressure can be beneficial (Imperiale, 2003). Therefore, a noninvasive metric for determining hepatic pressure and distinguishing it from the effect of advancing fibrosis stage would be clinically desirable. While hepatic stiffening reported due to advancing fibrosis stage has been suggested to occur due to increased fibrin and collagen deposition in the tissue (Yoneda et al., 2008; Friedrich-Rust et al., 2008), a nonlinear strain-based mechanism underlies hepatic stiffening observed with pressurization (Rotemberg et al., 2012). A novel experimental setup for determining concurrent SWS and axial strain estimates was designed and utilized to better understand the nonlinear hyperelastic properties of the pressurized liver.

In Fig. 5, the accumulation of axial strain estimates and 95% confidence interval can be observed for one pressurization increment. The summed 95% interval represents the confidence interval of the summed strain estimate.

SWS estimates were observed to increase from 1.5–2 m/s at 0–5 mmHg (baseline) to 3.25–3.5 m/s at 20 mmHg in 6 of the
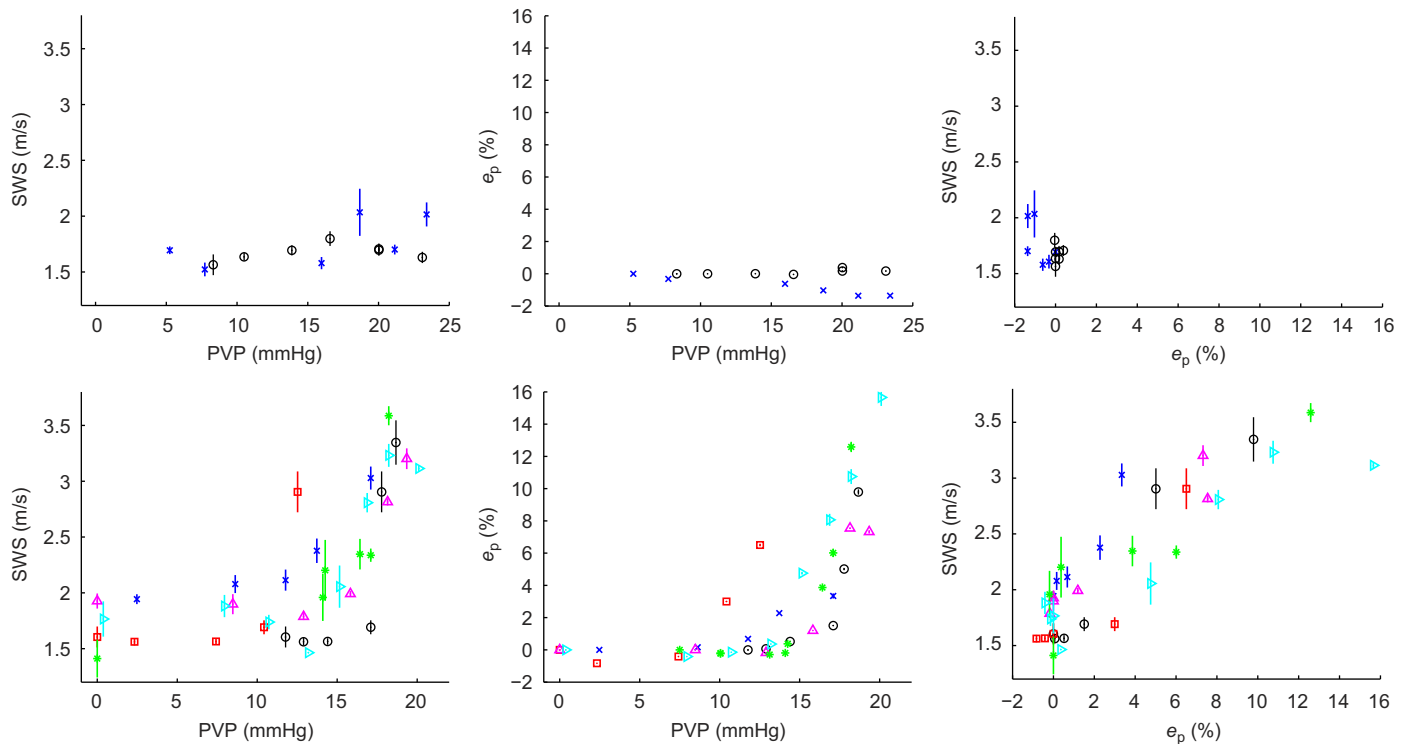
Fig. 6. Comparison between SWS, pressure, and axial strain for the 2 excised canine livers that were not observed to expand (top row) and for the 6 excised canine livers for which SWS and axial strain were observed to increase with portal venous pressure. SWS measures were compared with portal venous pressure (left column) and axial strain measures (right column). Because the 6 SWS estimates were in the same region of interest, the error bars (which represent the standard deviation of the 6 SWS estimates) do not show potential tissue heterogeneity but rather the limits of system precision on SWS estimates. Axial strain measures were compared with portal venous pressure (center column). The error bars shown represent the summed 95% confidence interval on the strain estimate.

8 canine livers interrogated. SWS measures at baseline varied between 1.4 and 2 m/s in the livers tested. While this result is consistent with reported variability in healthy human livers (Roulot et al., 2008), it may be that this difference may reflect a difference in underlying hepatic material properties or state of stress that would affect the response of the liver to applied portal pressure. This remains to be further investigated from the perspective of selecting either a nonlinear model to encompass the behavior of all healthy livers or choosing a class of models that should be fit to each liver individually in future work.

When portal venous pressure was increased from clinically normal (0–5 mmHg) to pressures representing highly diseased states at 20 mmHg, axial strain was observed to increase up to 10%. Between 0 and 10 mmHg, some estimates of axial strain were observed to decrease slightly (up to 1%). It is possible that the static pressure in the saline bath around the liver plays a confounding role in the experiment. If that is the case, when the portal vein pressure is lower than the external static pressure, the liver may appear to decrease in size.

Although there was a clear correlation between increasing strain and SWS, there was variability among the different livers. We hypothesize that some of the variability in SWS increase as a result of elevating PVP may be a result of different strains achieved in different livers at the same pressure. For example, the canine liver corresponding to the red squares clearly has a lower pressure at which an increase in SWS and percent axial strain were observed but appear consistent with the relationship between SWS and percent axial strain seen in the other hepatic cases (Fig. 6). This result is likely due to the pressure behaving differently on livers with different geometries and supports the use of strain and SWS measures for quantifying tissue nonlinear behavior. The complex geometry of the liver does not allow use of the relationship between pressure and strain or stiffness to directly

generate predictions of nonlinear behavior. In addition, the increases in SWS corresponding to axial strain increases of 4% above baseline configuration suggest that a transition between where a linear model may be sufficient to states in which nonlinear regimes dominate occurs at smaller strain states in these data than the greater than 10% strain that is classically assumed to correspond to nonlinear hyperelastic behavior (Lai et al., 1999).

In two of the livers examined, neither expansion in the form of axial strain increase nor stiffening was observed. Fig. 6 shows these results. This lack of expansion and stiffening still supports our hypothesis that deformation is required in order to observe SWS increases. In one of the cases, heparin was not administered prior to euthanasia, so we hypothesize that clotting effects prevented the pressurization from communicating throughout the liver. In the other case, it is possible that a small defect in the liver capsule or air in the portal venous system prevented the distribution of the increasing PVP throughout the liver. It is unlikely that air, excessive clotting, or capsule defects would exist when interrogating increasing PVP in vivo, but the fact that even in those cases the SWS and expansion of the liver were correlated continues to support the use of a strain-dependent model for the effect of hepatic pressure on stiffness metrics.

Increases in measurements of hepatic axial strain were associated with increases in concurrently acquired SWS estimates. Fig. 6 shows the relationship between the accumulated axial strain at a given pressure and the average of 6 SWS estimates generated at each pressurization step. This data provides the correlation between SWS and strain, which will be used moving forward to generate nonlinear material models of hepatic tissues. A limitation of this initial study is that we used only healthy canine livers for the experiment. Because most patients who suffer from elevated PVP have advanced liver disease, it will also be important to explore the effect of cirrhosis on hepatic nonlinear behavior.

In particular, pressure will be expected to have a smaller effect on hepatic strain in stiffer livers of cirrhotic patients. In the clinical setting, a fully characterized nonlinear tissue model may require two stiffness measures at different strain or pressurization stages in order to characterize underlying hepatic mechanics. A potential method for gaining this information would be to generate two estimates of strain and SWS before and after external compression. The relationship between the change in strain state with compression and shear wave speed could provide the basis for determining the hepatic fibrosis stage and pressurization state noninvasively.

Initial results suggest that hyperelastic material modeling of the liver on the basis of the correlation between SWS and axial strain is possible and appropriate and may provide the basis for a nonlinear mechanical model that leads to an improved understanding of liver stiffening with disease-associated portal venous pressure increases.

6. Conclusions

This work shows that increasing shear wave speed estimates with hepatic pressurization are associated with increases in hepatic axial strain, and quantifies these behaviors. Increases from normal portal venous pressure to diseased (an increase from about 0 to 20 mmHg) were associated with a deformation of up to 10% axial strain and up to a 2.3 multiplicative increase in liver shear wave speed estimate from baseline in normal canine livers. These results provide a foundation for hyperelastic material modeling of the liver.

Conflict of interest statement

Two of the authors: Kathryn Nightingale and Mark Palmeri, hold patents based upon the Acoustic Radiation Force Impulse (ARFI) technology that served as the basis of hepatic stiffness (ultrasonic shear wave speed) characterization in this work.

I also confirm that we have given due consideration to the protection of intellectual property associated with this work and that there are no impediments to publication, including the timing of publication, with respect to intellectual property. We have followed the regulations of our institutions concerning intellectual property in submitting this work.

I further confirm that any aspect of the work covered in this manuscript that has involved either experimental animals or human patients has been conducted with the ethical approval of all relevant bodies and that such approvals are acknowledged within the manuscript.

Acknowledgments

References

Bavu, E., Gennisson, J.L., Couade, M., Bercoff, J., Mallet, V., Fink, M., Badel, A., Vallet-Pichard, A., Nalpas, B., Tanter, M., Pol, S., 2011. Noninvasive in vivo liver fibrosis evaluation using supersonic shear imaging: a clinical study on 113 hepatitis C virus patients. Ultrasound in Medicine & Biology 37, 1361–1373.

Bolondi, Luigi, Gaiani, Stefano, 1994. The relationship of endoscopy, portal Doppler ultrasound flowmetry, and clinical and biochemical tests in cirrhosis. Journal of Hepatology 20, 11–18.

Bolondi, Luigi, Gaiani, Stefano, Barbara, Luigi, 1991. Accuracy and reproducibility of portal flow measurement Doppler US. Journal of Hepatology 13, 269–273.

Brunon, A., Bruyère-Garnier, K., Coret, M., 2010. Mechanical characterization of liver capsule through uniaxial quasi-static tensile tests until failure. Journal of Biomechanics 43, 2221–2227.

Bureau, C., Metivier, S., Peron, J.M., Selves, J., Robic, M.A., Gourraud, P.A., Rouquet, O., Dupuis, E., Alric, L., Vinel, J.P., 2008. Transient elastography accurately predicts presence of significant portal hypertension in patients with chronic liver disease. Alimentary Pharmacology and Therapeutics 27, 1261–1268.

Byram, Brett, Holley, Greg, Giannantonio, Doug, Trahey, Gregg, 2010. 3-D phantom and in vivo cardiac speckle tracking using a matrix array and raw echo data. IEEE Transactions on Ultrasonics, Ferroelectrics, and Frequency Control 57, 839–854.

Crespo, Gonzalo, Fernández-Varo, Guillermo, Mariño, Zoe, Casals, Gregori, Miquel, Rosa, Martínez, Stella M., Gilabert, Rosa, Forns, Xavier, Jiménez, Wladimiro, Navasa, Miquel, 2012. ARFI, FibroScan, ELF, and their combinations in the assessment of liver fibrosis: a prospective study. Journal of Hepatology 57, 281–287.

Embree, P.M., O'Brien, W.D., 1985. The accurate ultrasonic measurement of the volume flow of blood by time domain correlation. IEEE Ultrasonics Symposium, 963–966.

Frey, Gregg, Chiao, Richard, 2008. 4Z1c real-time volume imaging transducer ACUSON SC2000 volume imaging ultrasound system 4Z1c real-time volume imaging transducer. Whitepaper, 1–6.

Friedrich-Rust, M., Ong, M.F., Martens, S., Sarrazin, C., Bojunga, J., Zeuzem, S., Herrmann, E., 2008. Performance of transient elastography for the staging of liver fibrosis: a meta-analysis. Gastroenterology 134, 960–974.

Gennisson, J.-L., Rénier, M., Catheline, S., Barrière, C., Bercoff, J., Tanter, M., Fink, M., 2007. Acoustoelasticity in soft solids: assessment of the nonlinear shear modulus with the acoustic radiation force. Journal of the Acoustical Society of America 122, 3219.

Gulzar, G.M., Zargar, S.A., Jalal, S., Alaie, M.S., Javid, G., Suri, P.K., Bilal-Ul-Rehman Shah, N.A., Hakeem, M.S., Shoukat, A., Dar, G.A., 2009. Correlation of hepatic venous pressure gradient with variceal bleeding, size of esophageal varices, etiology, acites and degree of liver dysfunction in cirrhosis of liver. Indian Journal of Gastroenterology 28, 61.

Han, J.-Y., Cho, J.H., Kwon, H.J., Nam, K.J., 2012. Predicting portal hypertension as assessed by acoustic radiation force impulse: correlations with the Doppler ultrasound. British Journal of Radiology 85, e404–e409.

Hjelmstad, Keith, 2005. Fundamentals of Structural Mechanics. 2. Springer Science, New York.

Imperiale, T., 2003. Measuring the hemodynamic response to primary pharmaco-prophylaxis of variceal bleeding: a cost-effectiveness analysis. American Journal of Gastroenterology 98, 2742–2750.

Jordan, P., Socrate, S., Zickler, T.E., Howe, R.D., 2009. Constitutive modeling of porcine liver in indentation using 3D ultrasound imaging. Journal of the Mechanical Behavior of Biomedical Materials 2, 192–201.

Kallel, F., Bertrand, M., Ophir, J., 1996. Fundamental limitations on the contrast-transfer efficiency in elastography: an analytic study. Ultrasound in Medicine and Biology 22, 470.

Kallel, F., Ophir, J., 1997. A least-squares strain estimator for elastography. Ultrasonic Imaging 19, 195–208.

Konofagou, Elisa, Lee, Wei-Ning, Luo, Jianwen, Provost, Jean, Vappou, Jonathan, 2011. Physiologic cardiovascular strain and intrinsic wave imaging. Annual Review of Biomedical Engineering 13, 1241–1254.

Korukonda, Sanghamithra, Doyley, Marvin M., 2011. Estimating axial and lateral strain using a synthetic aperture elastographic imaging system. Ultrasound in Medicine & Biology 37, 1893–1908.

Kuo, Johnny, von Ramm, Olaf T., 2008. Three-dimensional motion measurements using feature tracking. IEEE transactions on ultrasonics, ferroelectrics, and frequency control 55, 800–810.

Lai, W.M., Rubin, D., Kremple, E., 1999. Introduction to Continuum Mechanics.

Loupas, T., Peterson, R., Gill, R., 1995. Experimental evaluation of velocity and power estimation for ultrasound blood flow imaging, by means of a two-dimensional autocorrelation approach. IEEE Transactions on Ultrasonics, Ferroelectrics and Frequency Control 42, 689–699.

Millonig, Gunda, Friedrich, Stefanie, Adolf, Stefanie, Fonouni, Hamidreza, Golriz, Mohammad, Mehrabi, Arianeb, Stiefel, Peter, Pöschl, Gudrun, Büchler, Markus W., Karl Seitz, Helmut, Mueller, Sebastian, Poschl, G., Buchler, M., 2010. Liver Stiffness is directly influenced by central venous pressure. Journal of Hepatology 52, 206–210.

Nedredal, G.I., Yin, M., McKenzie, T., Lillegard, J., Luebke-Wheeler, J., Talwalkar, J., Ehman, R., Nyberg, S.L., 2011. Portal hypertension correlates with splenic stiffness as measured with MR elastography. Journal of Magnetic Resonance Imaging 34, 79–87.

Nicolle, S., Vezin, P., Palierne, J.F., 2010. A strain-hardening bi-power law for the nonlinear behaviour of biological soft tissues. Journal of Biomechanics 43, 927–932.

Nightingale, K.R., McAleavey, S.A., Trahey, G.E., 2003. Shear wave generation using acoustic radiation force: in vivo and ex vivo results. Ultrasound in Medicine and Biology 29, 1723.

Palmeri, M.L., Wang, M.H., Dahl, J.J., Frinkley, K.D., Nightingale, K.R., 2008. Quantifying hepatic shear modulus in vivo using acoustic radiation force. Ultrasound in Medicine and Biology 34, 546–558.

Palmeri, Mark L., Wang, Michael H., Rouze, Ned C., Abdelmalek, Manal F., Guy, Cynthia D., Moser, Barry, Mae Diehl, Anna, Nightingale, Kathryn R., 2011. Noninvasive evaluation of hepatic fibrosis using acoustic radiation force-based

shear stiffness in patients with nonalcoholic fatty liver disease. Journal of hepatology 55, 666–672.

Pinton, Gianmarco F., Dahl, Jeremy J., Trahey, Gregg E., 2006. Rapid tracking of small displacements with ultrasound. IEEE Transactions on Ultrasonics Ferroelectrics and Frequency Control 53, 1103–1117.

Righetti, Raffaella, Srinivasan, Seshadri, Ophir, Jonathan, 2003. Lateral resolution in elastography. Ultrasound in Medicine & Biology 29, 695–704.

Ripoll, C., Groszmann, R., Garcia-Tsao, G., Grace, N., Burroughs, A., Planas, R., Escorsell, A., Garcia-Pagan, J.C., Makuch, R., Patch, D., Matloff, D.S., Bosch, J., 2007. Hepatic venous pressure gradient predicts clinical decompensation in patients with compensated cirrhosis. Gastroenterology 133, 488.

Robic, M.A., Procopet, B., Metivier, S., Peron, J.M., Selves, J., Vinel, J.P., Bureau, C., 2011. Liver Stiffness accurately predicts portal hypertension related complications in patients with chronic liver disease: a prospective study. Journal of Hepatology 55, 1017–1024.

Rotemberg, V., Palmeri, M., Nightingale, R., Rouze, N., Nightingale, K., 2012. The impact of hepatic pressurization on liver shear wave speed estimates in constrained versus unconstrained conditions. Physics in Medicine and Biology 57, 329–341.

Roulot, D., Czernichow, S., Clesiau, H.L., Costes, J.L., Vergnaud, A.C., Beaugrand, M., 2008. Liver stiffness values in apparently healthy subjects: Influence of gender and metabolic syndrome. Journal of Hepatology 48, 613.

Sandrin, Laurent, Tanter, Mickaël, Catheline, Stefan, Fink, Mathias, 2002. Shear modulus imaging with 2-D transient elastography. IEEE Transactions on Ultrasonics, Ferroelectrics and Frequency Control 49, 426–435.

Sarvazyan, A., Rudenko, O., Swanson, S., Fowlkes, J., Emelianov, S., 1998. Shear wave elasticity imaging: a new ultrasonic technology of medical diagnostics. Ultrasound in Medicine and Biology 24, 1435.

Schlosser, B., Biermer, M., Fulop, B., Schott, E., Asbach, P., Sack, I., Berg, T., 2009. Evaluation of Magnetic Resonance Elastography (MRE) as a non-invasive method to assess the stage of liver fibrosis in patients with chronic liver diseases. Hepatology 50, 919.

Shams, M.A., Destrade, M., Ogden, R.W., 2011. Initial stresses in elastic solids: constitutive laws and acoustoelasticity. Wave Motion 48, 552–567.

Sharara, Ala I., Rockey, D.C., 2001. Gastroesophageal Variceal Hemorrhage. New England Journal of Medicine 345, 669–681.

Takuma, Yoshitaka, Nouso, Kazuhiro, Morimoto, Youichi, Tomokuni, Junko, Sahara, Akiko, Toshikuni, Nobuyuki, Takabatake, Hiroyuki, Shimomura, Hiroyuki, Doi, Akira, Sakakibara, Ichiro, Matsueda, Kazuhiro, Yamamoto, Hiroshi, 2013. Measurement of spleen stiffness by acoustic radiation force impulse imaging identifies cirrhotic patients with esophageal varices. Gastroenterology 144(1), 92–101.

Vizzutti, F., Arena, U., Rega, L., Pinzani, M., 2008. Non invasive diagnosis of portal hypertension in cirrhotic patients. Gastroenterologie Clinique et Biologique 32, 87.

Vries, P.J. de, van Hatturn, J., Hoekstra, J.B.L., de Hooge, P., 1991. Duplex Doppler measurements of portal venous Slow in normal subjects. Journal of Hepatology 13, 358–363.

Wang, M.H., Palmeri, M.L., Rotemberg, V.M., Rouze, N.C., Nightingale, K.R., 2010. Improving the robustness of time-of-flight based shear wave speed reconstruction methods using RANSAC in human liver in vivo. Ultrasound in Medicine and Biology 36, 802–813.

Wang, Shougang, Lee, Wei-Ning, Provost, Jean, Luo, Jianwen, Konofagou, Elisa E., 2008. A composite high-frame-rate system for clinical cardiovascular imaging. IEEE Transactions on Ultrasonics, Ferroelectrics, and Frequency Control 55, 2221–2233.

Wear, K.A., Popp, R.L., 1987. Theoretical analysis of a technique for the characterization of myocardium contraction based upon temporal correlation of ultrasonic echoes. IEEE Transactions on Ultrasonics, Ferroelectrics, and Frequency Control 34, 368–375.

Wu, Chung-Chieng, 2008. Ultrasonographic evaluation of portal hypertension and liver cirrhosis. Journal of Medical Ultrasound 16, 188–193.

Yang, Sien-sing, 2007. Duplex Doppler ultrasonography in portal hypertension. Journal of Medical Ultrasound 15, 103–111.

Yin, M., Kolipaka, A., Woodrum, D.A., Glaser, K.J., Romano, A.J., Manduca, A., Talwalkar, J.A., Araoz, P.A., McGee, K.P., Anavekar, N.S., Ehman, R.L., 2011. Hepatic and splenic stiffness augmentation assessed with MR elastography in an in vivo porcine portal hypertension model. American Journal of Roentgenology 197(1), 64–70.

Yoneda, M., Mawatari, H., Fujita, K., Endo, H., Lida, H., Nozaki, Y., Yonemitsu, K., Higurashi, T., Takahashi, H., Kobayashi, N., Kirikoshi, H., Abe, Y., Inamori, M., Kubota, K., Saito, S., Tamano, M., Hiraishi, H., Maeyama, S., Yamaguchi, N., Togo, S., Nakajima, A., 2008. Noninvasive assessment of liver fibrosis by measurement of stiffness in patients with nonalcoholic fatty liver disease (NAFLD). Digestive and Liver Disease 40, 378.

Zironi, Gianni, Gaiani, Stefano, Rigamonti, Alessandra, Bolondi, Luigi, Barbara, Luigi, 1992. Value of measurement of mean portal flow velocity by Doppler flowmetry in the diagnosis of portal hypertension. Journal of Hepatology 16, 298–303.